ADVANCES IN ATMOSPHERIC SCIENCES, VOL. 33, FEBRUARY 2016, 164–174

Trends of Regional Precipitation and Their Control Mechanisms during 1979–2013

Run LIU[1], Shaw Chen LIU[*2,3], Chein-Jung SHIU[2], Jun LI[1], and Yuanhang ZHANG[1]

[1]*State Key Joint Laboratory of Environmental Simulation and Pollution Control, College of Environmental Sciences and Engineering, Peking University, Beijing* 100871

[2]*Research Center for Environmental Changes, Academia Sinica, Taipei* 11529

[3]*Department of Atmospheric Science, NCU, Jhongli* 32001

(Received 13 May 2015; revised 5 August 2015; accepted 5 August 2015)

ABSTRACT

Trends in precipitation are critical to water resources. Considerable uncertainty remains concerning the trends of regional precipitation in response to global warming and their controlling mechanisms. Here, we use an interannual difference method to derive trends of regional precipitation from GPCP (Global Precipitation Climatology Project) data and MERRA (Modern-Era Retrospective Analysis for Research and Applications) reanalysis in the near-global domain of 60°S–60°N during a major global warming period of 1979–2013. We find that trends of regional annual precipitation are primarily driven by changes in the top 30% heavy precipitation events, which in turn are controlled by changes in precipitable water in response to global warming, i.e., by thermodynamic processes. Significant drying trends are found in most parts of the U.S. and eastern Canada, the Middle East, and eastern South America, while significant increases in precipitation occur in northern Australia, southern Africa, western India and western China. In addition, as the climate warms there are extensive enhancements and expansions of the three major tropical precipitation centers–the Maritime Continent, Central America, and tropical Africa–leading to the observed widening of Hadley cells and a significant strengthening of the global hydrological cycle.

Key words: regional precipitation, global warming, water resources

Citation: Liu, R., S. C. Liu, C.-J. Shiu, J. Li, and Y. Zhang, 2016: Trends of regional precipitation and their control mechanisms during 1979–2013. *Adv. Atmos. Sci.*, **33**(2), 164–174, doi: 10.1007/s00376-015-5117-4.

1. Introduction

Considerable uncertainty remains concerning the magnitude and regional differences of trends in precipitation in response to global warming. In a warming climate, the saturation water vapor pressure will increase with atmospheric temperature according to the Clausius–Clapeyron equation (CC) at about 7% K^{-1}. This rate of increase with temperature has been substantiated by radiosonde measurements (Durre et al., 2009; Dai et al., 2011), as well as in trends of column water vapor density (Trenberth et al., 2005; Santer et al., 2007). Meanwhile, the global mean precipitation or global evaporation that is controlled by the surface energy budget does not scale with CC, increasing at around 2% K^{-1} (Cubasch et al., 2001; Allen and Ingram, 2002). Analysis of two long-term gauge-based precipitation datasets over land showed that the annual average global total precipitation of both datasets had small linear increasing trends, but not statistically significant (Vose et al., 1992; Mitchell and Jones, 2005; Trenberth et al., 2007), consistent with the predicted small increase in global precipitation/evaporation in response to global warming. This is also consistent with precipitation data from the Global Precipitation Climatology Project, version 2.2 (GPCP V2.2), in the near-global domain of 60°S–60°N analyzed in this work, of which the annual total precipitation of the entire domain decreases by an insignificant 0.66% (P-value = 0.3) during the period 1979–2013.

To analyze the regional distributions of precipitation changes, a useful framework consists of decomposing them into a part that is related to atmospheric circulation changes and a part that is related to water vapor changes, referred to as dynamic and thermodynamic components, respectively. However, definitions of these two components may differ among studies, partly because there are significant overlaps and interactions between the two components.

There is a relatively sound physical basis for the drying of the dry subtropics (i.e., the "dry-get-drier" mechanism) and increased precipitation in the wet intertropical convergence zone (ITCZ) (i.e., "wet-get-wetter") as global temperatures rise (Mitchell et al., 1987; Held and Soden, 2006; Chou et al., 2013). Assuming circulation remains the same, the in-

* Corresponding author: Shaw Chen LIU
Email: shawliu@gate.sinica.edu.tw

crease of lower tropospheric water vapor with temperature leads to more moisture convergence, more latent heat release, stronger convection, more precipitation than CC, and removal of more water vapor than CC in the ascending/wet zones; while in the descending/dry zones, there is additional moisture divergence and less water vapor than CC, resulting in less precipitation.

Observed widening of the Hadley cell due to global warming (Hu and Fu, 2007; Zhou et al., 2011; Davis and Rosenlof, 2012) implies the expansion of subtropical dry zones and broader tropical rain belts, probably leading to drier subtropical dry zones and wetter tropics, respectively. These changes are generally consistent with the wet-get-wetter and dry-get-drier mechanism (WWDD) (Zhou et al., 2011; Chou et al., 2013). In model projections, there are indications of a weakening of the tropical overturning of air as the climate warms (Held and Soden, 2006; Vecchi and Soden, 2007; Chadwick et al., 2013). But, there is no conclusive evidence for the implied slowdown of the Hadley (Stachnik and Schumacher, 2011; Zhou et al., 2011) or Walker circulations (Vecchi et al., 2006; Zhou et al., 2011; Tokinaga et al., 2012).

Increases in latent heat release in storms due to the increased moisture with temperature can invigorate the storms and produce heavier precipitation. The increase in heavy precipitation from an invigorated storm can exceed the CC value (thermodynamic process), and remove more moisture from the atmosphere than 7% K^{-1}, resulting in less light and moderate precipitation on the global scale (Trenberth et al., 2003). Moreover, a reduced lapse rate in a warmer climate (Held and Soden, 2006; Dessler and Davis, 2010) can make the atmosphere more stable and thus less likely to precipitate (dynamic process), especially for light and moderate precipitation that requires an unstable large-scale environment. The combined result of increased heavy precipitation and suppressed light and moderate precipitation is an increase in precipitation intensity, which has been substantiated by analyses of observed precipitation from GPCP, TRMM (Tropical Rainfall Measuring Mission), as well as some reanalyses (Liu et al., 2009; Lau and Wu, 2011; Shiu et al., 2012). Results from climate models also show a significant increase in precipitation intensity, albeit substantially smaller than observed increases (Sun et al., 2007). This mechanism will result in "heavy-precipitation-get-heavier" and "light-precipitation-get-lighter" (HHLL) trends in the total precipitation in response to global warming.

In the context of the regional distribution of trends in precipitation in response to global warming, HHLL would lead to more precipitation in regions dominated by heavy precipitation (e.g., the ITCZ, South Pacific convergence zone, and storm tracks of tropical storms), and less precipitation in regions dominated by light and moderate precipitation (e.g., the descending zones of Hadley cells). So, there can be considerable but not necessarily complete overlaps of regions affected by HHLL and WWDD, as wet areas can also have light precipitation and dry areas can have heavy precipitation.

The major objectives of this study are to evaluate the trends of regional precipitation in response to global warming and to identify the primary controlling mechanism(s) of these trends. We will examine data from GPCP V2.2 (Adler et al., 2003) and MERRA (Modern-Era Retrospective Analysis for Research and Applications) reanalysis (Rienecker et al., 2011) in the near-global domain of 60°S–60°N during a major global warming period of 1979–2013. Results using other reanalysis data, such as ERA-Interim (European Centre for Medium-Range Weather Forecasts Interim Reanalysis) (Fig. S1, only available online) and NCEP/NCAR R1 (National Centers for Environmental Prediction/National Center for Atmospheric Research Reanalysis 1) (Fig. S2), are similar to those of MERRA, and thus only presented as supplementary material. In the methodology section, we compare the interannual difference method (IDM) to two other different methods for evaluating the trends of precipitation; namely, a linear time series method (LTSM) and a linear scatter correlation method (LSCM). As a demonstration, the three methods are used to evaluate the trend of precipitation at an arbitrarily chosen equatorial grid point in the Maritime Continent (MC) of GPCP V2.2 data. Mutually consistent results are obtained, and the advantages and limitations of the IDM are discussed. The IDM is then applied to all individual grids in the domain of 60°S–60°N to study the trends of regional precipitation in response to global warming. Finally, we compare the HHLL to WWDD to determine which mechanism is the primary driving force in the control of the regional changes of annual precipitation in response to global warming.

2. Data and Methods

Data from GPCP V2.2 ($2.5° \times 2.5°$, monthly, 1979–2013) (Adler et al., 2003) are used in this study. Data from the MERRA reanalysis (Rienecker et al., 2011) and the Global Precipitation Climatology Centre (GPCC, Full Data Reanalysis Version 6.0, $2.5° \times 2.5°$, monthly, 1901–2010) (Schneider et al., 2014) are also analyzed to check the robustness of our results. Surface air temperature is taken from the Global Historical Climatology Network-Monthly dataset, version 3.2.1 (Jones and Moberg, 2003). SST is taken from the Extended Reconstructed Sea Surface Temperature dataset, version 3b (Smith et al., 2008). The global mean temperature anomaly (relative to the 1901–2000 base period) is taken from the National Climatic Data Center (available at http://www.ncdc.noaa.gov/cag/time-series/global/globe/land_ocean/ytd/12/1880-2014.csv).

Figure 1a shows temporal variations of the annual total precipitation (from GPCP V2.2) at an arbitrarily chosen equatorial grid point (3.75°S, 141.25°E) in the MC, and the global annual mean temperature anomaly for the period 1979–2013. The global temperature anomaly instead of the local temperature anomaly is used here for the following reason: According to the thermodynamic hypothesis, the temperature used in the data analysis should be the atmospheric temperature of the region from which the bulk of water vapor of the precipitation originates. For the equatorial grid point chosen, the temperature should be the air temperature over a synop-

tic scale region in the MC. Since we are dealing with large spatial and temporal (yearly) average phenomena, the atmospheric temperature of the region tends to change proportionally with the global surface temperature with a near unit ratio. For example, the ratio of temperature anomalies between the 10°S–10°N oceanic region and the near-global zone is about 0.93. Thus, for convenience, global temperature can be used as a proxy.

Since there is an obvious correlation between the precipitation and temperature, statistically, a significant value can be derived for the change of precipitation as a function of the temperature anomaly, i.e. $\Delta P/\Delta T$, where P denotes precipitation and T the temperature. Under the assumption of a linear causal relationship between P and T, $\Delta P/\Delta T$ can be interpreted as the change in the annual total precipitation at the grid point in response to a one degree Kelvin increase in the global mean temperature. Three methods for calculating $\Delta P/\Delta T$ are evaluated in this study: LTSM, LSCM, and IDM. All three methods are based on the correlation between the precipitation and global mean temperature anomaly. As it is well known that a good correlation does not imply any causal relationship, none of the three methods can be claimed as the physically correct method. LTSM is the traditional and commonly used method; it physically assumes that both the precipitation and temperature are linearly dependent on time, and ΔP and ΔT are their linear trends for the entire period (blue and red dashed lines in Fig. 1a). Figure 1b shows the scatter correlation plot (LSCM) between the precipitation and global mean temperature anomaly. This plot ignores the time sequence of the precipitation or temperature; instead, the LSCM $\Delta P/\Delta T$ is calculated directly from the linear regression between the precipitation and global mean temperature anomaly. This is physically equivalent to assuming the annual precipitation is linearly dependent on the annual global mean temperature.

LSCM is different from LTSM in an important aspect: LTSM assumes a linear dependence on time for both the precipitation and the global mean temperature, while LSCM does not. By applying temporal linear regression, LTSM filters out nonlinear temporal variations in both the precipitation and the temperature anomaly, e.g., El Niño–Southern Oscillation (ENSO); while the nonlinear effects are retained, at least partially in LSCM. IDM (Fig. 1c) has been used successfully and described in detail in our previous works (Liu et al., 2009; Shiu et al., 2012). It is identical to LSCM, except that it improves upon the statistics by replacing individual points with their interannual differences, including differences between two years not adjacent to each other in time. Thus, it increases the number of independent data points by $(n-1)/2$, where n is the number of points in LSCM (35 points or years). The results from IDM and LSCM should converge when the number of data points increases. This is supported by the values of $\Delta P/\Delta T$ derived by the two methods for the equatorial grid: 1258 (±334) and 1205 (±138) for LSCM and IDM, respectively, which differ only by about 5% and are well within their standard errors of the mean (SEM, values in parentheses). The results from LTSM converge with those

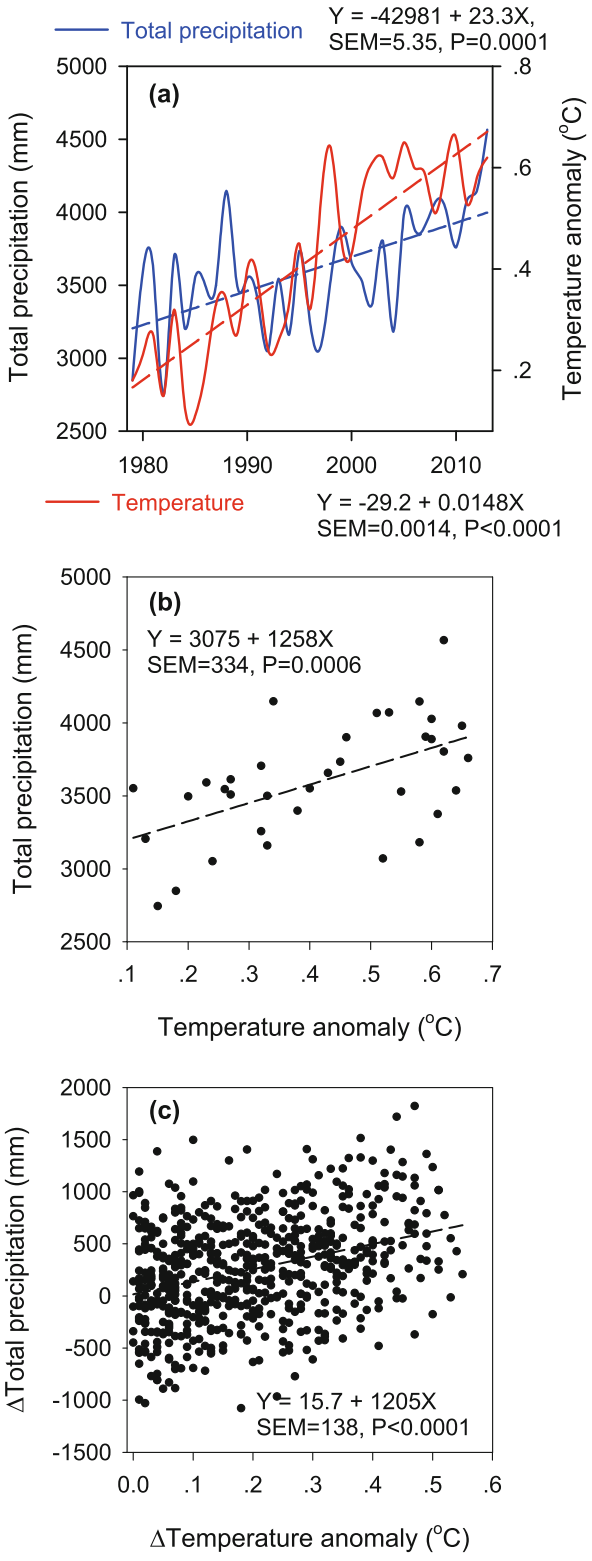

Fig. 1. (a) Temporal variations with linear regressions (dashed lines) of the annual total precipitation at an equatorial grid point (3.75°S, 141.25°E) and the annual global mean temperature anomaly (1979–2013). (b) Annual total precipitation plotted against the annual global mean temperature anomaly; the dashed line is the linear regression (LSCM). (c) The same as (b) except the absolute values are replaced by their interannual differences (IDM).

from IDM and LSCM only if both the precipitation and the temperature are linearly dependent on time. In reality, neither the precipitation nor the temperature is linearly dependent on time. Nevertheless, for the equatorial grid point, the value of $\Delta P/\Delta T$ derived by LTSM is 1572 ($\pm$511), consistent with those derived by the other two methods within their combined SEMs. This consistency is not unique to the equatorial grid. As demonstrated in the text and the supplementary material, the consistency prevails in widespread areas over the globe (Figs. 2 and S3).

The consistency among the three methods suggests that the trend of regional precipitation tends to respond to global warming in a quasi-linear manner, and either method can be used to derive the trend. Since IDM has the lowest value of SEM among the three methods, in this study we use IDM, but cross check with LTSM to ensure the robustness of the results.

Some words of caution are due here despite the remarkable consistency among the three methods over widespread areas of the globe. Consistent and reasonable answers for $\Delta P/\Delta T$ do not necessarily imply correct answers. Values of $\Delta P/\Delta T$ are observed or apparent slopes between P and T, which have been linearized by the three correlation methods. There is no particular reason to linearize the slope. It is done for simplicity and convenience. Moreover, while we will interpret the slope of $\Delta P/\Delta T$ as the change of precipitation due

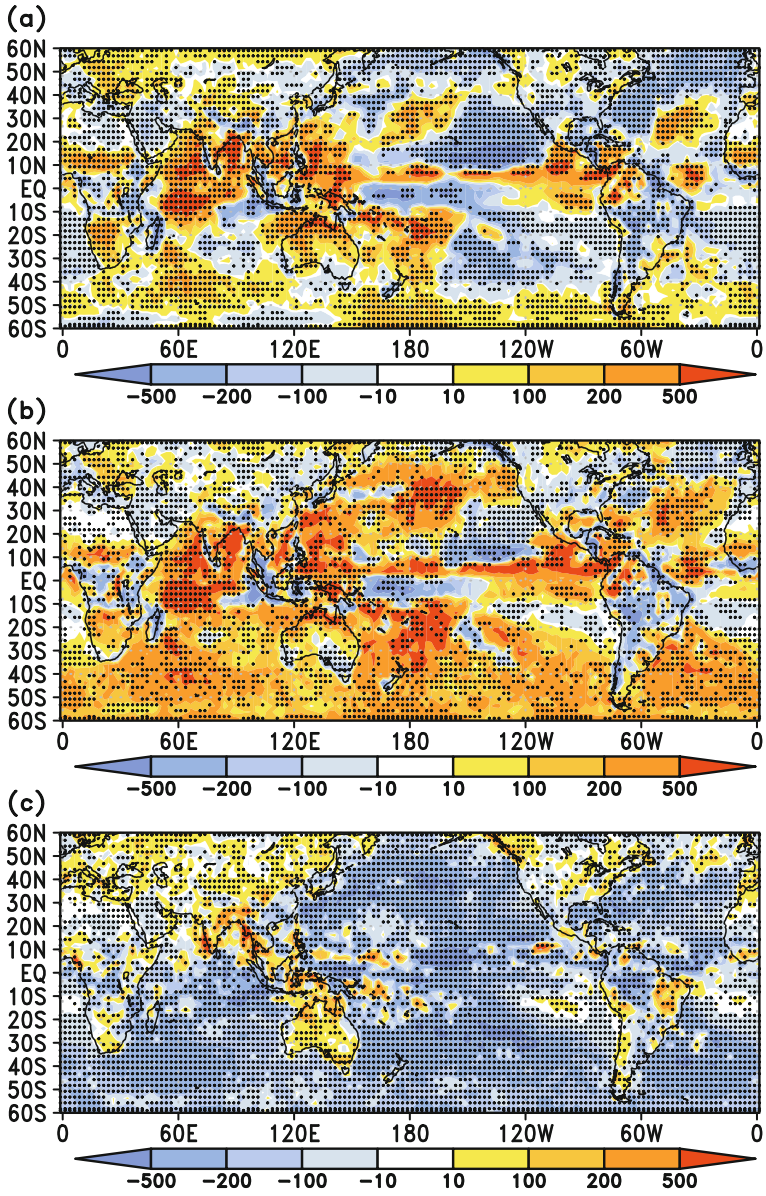

Fig. 2. (a) Trends in annual total precipitation (units: mm K^{-1}) in response to a one degree Kelvin warming in global mean temperature derived from GPCP V2.2 (1979–2013) by IDM. (b) As in (a) except for the top 30% heavy precipitation. (c) As in (a) except for the bottom 70% light and moderate precipitation. Crosses indicate changes significant at the 95% confidence level.

to a one degree Kelvin increase of global temperature, in reality other factors can also contribute to the slope, either positively or negatively. The interpretation is valid only when the value of the slope is substantiated by both theory and modeling results.

3. Trends of regional precipitation in the near-global domain of 60°S–60°N

IDM and LTSM are applied to individual grids of GPCP V2.2 (1979–2013) to study the trends of regional precipitation in response to global warming in a near-global domain of 60°S–60°N. Figure 2 shows the spatial distributions of $\Delta P/\Delta T$ for the annual total precipitation (Fig. 2a), top 30% heavy precipitation (Fig. 2b), and bottom 70% light and moderate precipitation (Fig. 2c). The ranges of the top 30% and bottom 70% at each grid are determined and fixed for the entire period of 1979–2013, as follows: Monthly GPCP V2.2 precipitation data at a resolution of $2.5^\circ \times 2.5^\circ$ for the entire period of 1979–2013 at an individual grid point are gathered together and sorted into 10 bins of equal precipitation amount in increasing precipitation intensity. The ranges of the 10 bins at each grid are determined by this sorting and fixed throughout the analysis. The precipitation amount within each bin at each grid for a given year is sorted in the same way, but with the fixed ranges of the entire period of 1979–2013.

As discussed in the methodology section, $\Delta P/\Delta T$ (in mm K^{-1}) can be interpreted as the trend of annual precipitation in response to a one degree Kelvin increase of annual global mean temperature. The mm K^{-1} units can be converted to mm $(10\ yr)^{-1}$ by multiplying by the value of 0.148 K $(10\ yr)^{-1}$, which is the linear rate of global warming in 1979–2013 (Fig. 1a). Areas marked with crosses in Fig. 2 denote grids for which the *P*-values are less than 0.05, i.e., within the 95% confidence level. It can be seen that areas with crosses account for a majority (about 60%) of the domain. In comparison, LTSM (Fig. S3) renders only about 30% of the domain within the 95% confidence level. Nonetheless, consistent with the discussion in the methodology section, the patterns in Fig. S3 are in good agreement with those in Fig. 2, especially for features within the 95% confidence levels in both figures. This agreement has a pivotal implication: since nonlinear temporal variations are filtered out by LTSM, the results from IDM, which are in agreement with those from LTSM, should also be free from any significant influence of nonlinear variations, such as those from ENSO, the Indian Ocean dipole etc. In the case of ENSO, this implied notion is supported by the correlation plot between the global mean temperature anomaly and an ENSO index, Niño3.4. Their slope turns out to be indistinguishable from zero, as the *P*-value for the linear regression is 0.87 (Fig. S4).

The trends in regional annual total precipitation, shown in Fig. 2a, agree well with results of previous studies (Adler et al., 2008; Zhou et al., 2011; Liu and Allan, 2013) in which LTSM analyses of GPCP V2.2 were performed. This agreement provides additional evidence for the credence of IDM. Actually, previous results are almost identical to those in Fig. S3a. For instance, the drying of the southwestern U.S. and Middle East, and the increase in precipitation in northern Australia, can also be seen in most previous work. Nevertheless, our use of IDM allows a more significant statistical quantification, and thus a more in-depth analysis of the regional changes, as compared to LTSM analyses.

4. Control mechanism of precipitation trends

A number of important pieces of new information can be deduced from Fig. 2. Firstly, Fig. 2b essentially contains all the increases in precipitation shown in Fig. 2a, in terms of both the regional distribution and magnitude of the trends. Nearly all increases in total precipitation can be attributed to increases in the top 30% heavy precipitation. In fact, increases in the top 10% heavy precipitation (Fig. 3) alone match very well with those of total precipitation. This implies that the results in this study are not sensitive to our choice of the 30% and 70% pairing; i.e., the pairing could be

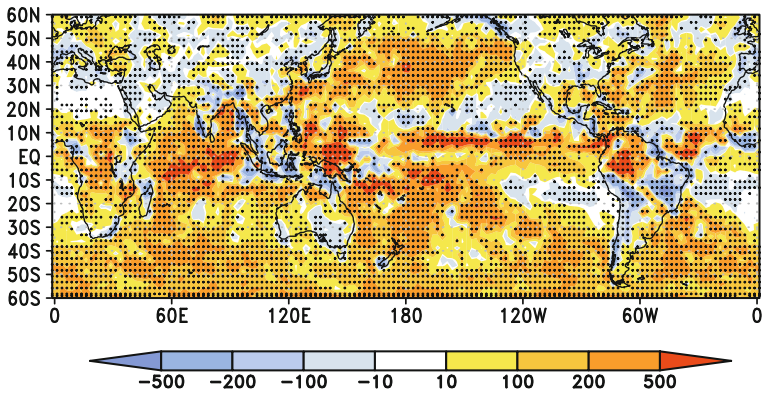

Fig. 3. Trends in the annual top 10% heavy precipitation (units: mm K^{-1}) in response to a one degree Kelvin warming in global mean temperature derived from GPCP V2.2 (1979–2013) by IDM. Crosses indicate changes significant at the 95% confidence level. The increasing trends match well with most of the increasing trends in total precipitation (Fig. 2a).

changed to 10% and 90%, or 40% and 60%, without significant effect on the results. Most of the significant decreases in total precipitation can also be attributed to the corresponding decreases in the top 30% heavy precipitation. For instance, decreases in the MC, Central and South America, tropical Africa, and the two descending/dry zones of Hadley cells in the eastern Pacific, can be seen in both Figs. 2a and b. Furthermore, increases in the top 30% heavy precipitation are significantly greater than those of total precipitation, particularly in spatial extent. Since the sum of all categories of precipitation intensity is constrained by the total precipitation of the entire domain, which, as mentioned earlier, decreases by an insignificant 0.66%, light and moderate precipitation must decrease significantly over large spatial areas. This is substantiated in Fig. 2c, which depicts relatively uniform reductions in the bottom 70% light and moderate precipitation over most of the oceanic areas. Over land, the bottom 70% light and moderate precipitation shows scattered increases, especially in the midlatitudes of the Northern Hemisphere and land areas in the MC. In summary, we find that the trends of regional annual total precipitation in response to global warming during the period 1979–2013 are primarily driven by the trends of the top 30% heavy precipitation, i.e., driven by the HH component of the HHLL mechanism.

Since monthly data are used, this finding that the changes in the top 30% heavy precipitation are in control implies that the trends of regional annual total precipitation in response to global warming during the period 1979–2013 are primarily driven by the trends of one to three months of heavy precipitation. In fact, the trends of annual total precipitation (Fig. 2a) match well with those of the top 10% heavy precipitation (Fig. 3), suggesting that the increasing trend of one single month of heavy precipitation is the primary contributor to the increasing trend of regional annual total precipitation in response to global warming during the period 1979–2013. This raises a concern that the monthly resolution of GPCP V2.2 is too coarse, and the finding may be different if data of higher temporal resolution are used. However, this concern is alleviated by the fact that the trends derived from GPCP V2.2 (monthly) are shown to be in excellent agreement with those derived from GPCP V1.0 (pentad) for their overlapping period of 1979–2007 (Fig. S5). The fact that the trends tend to be greater, and the statistics better, for the higher resolution pentad data, has been fully addressed previously (Liu et al., 2009; Shiu et al., 2012).

A key validation for the HHLL mechanism can be seen in Figs. 4a–c, which are identical plots to Figs. 2a–c, respectively, except that they are derived from MERRA reanalysis for the same time period. Comparison of the GPCP results to those of the reanalysis is highly valuable because the precipitation from the reanalysis is not assimilated from observed precipitation, but from a model-calculated quantity that depends on parameterized moist convection and large-scale precipitation processes in the models used in the reanalysis. These parameterizations are similar to those of coupled climate models, but the atmospheric states (pressure, temperature, humidity, and winds, but not precipitation) are constrained by observations assimilated in the reanalysis. Therefore, the comparison constitutes an independent evaluation by climate models of the changes in precipitation derived from GPCP. The general agreement between Figs. 4a–c and Figs. 2a–c suggests that the major characteristics of Figs. 2a–c are robust, and possess a high degree of credibility.

But what drives the HHLL mechanism or the trends of the top 30% heavy precipitation? The trends of the upward moist convective mass flux (CMFMC, see supplement) should provide some key clues if thermodynamic processes are the primary driving force. Figure 5a shows the trends in the annual mean CMFMC in response to a one degree Kelvin increase in global mean temperature, derived by IDM from MERRA (1979–2013). The overwhelming increases in the CMFMC in the tropical zone (30°S–30°N) are clearly caused by increases in precipitable water, i.e., following CC (Fig. S6), and greater latent heat releases in response to global warming. Comparison of Fig. 5a to Figs. 4a and b indicates that their general patterns match each other very well, particularly in the tropics (30°S–30°N). For instance, the extensive enhancements/expansions of precipitation centers in the MC and Central America, and the expansion of the tropical African rain belt, are well matched among the three figures. Even the narrow decreasing trend from Indonesia to southern China is present in all three figures. This is particularly significant considering that Fig. 5a is a model product. As the CMFMC represents a key thermodynamic process, the agreement among Figs. 5a, 4a and b provides a piece of convincing evidence for the notion that thermodynamic processes are the primary driving force for the HHLL mechanism.

Regarding the cause of the trends in the bottom 70% light and moderate precipitation, there is an obvious compensating effect on the trends of the top 30% heavy precipitation, as shown in Figs. 2b and c, and Figs. 4b and c. In fact, Fig. 4c is almost a mirror image of Fig. 4b, but opposite in sign. The only obvious exceptions are the two descending zones of the Hadley cell in the eastern Pacific, which are negative in both figures, as discussed earlier. Thus, we conclude that the trends of the bottom 70% light and moderate precipitation are driven primarily by this compensating effect to the trends of the top 30% heavy precipitation.

Changes in the atmospheric lapse rate (dynamic process) (Held and Soden, 2006; Dessler and Davis, 2010) mentioned earlier can affect precipitation significantly, especially light and moderate precipitation. The trends of the lapse rates between the 700 hPa and surface air in response to global warming are presented in Fig. S7, which is also derived from MERRA. There are extensive reductions in lapse rates (yellow and red areas, positive values) over the ocean, but mostly increases in lapse rates over land. Such a pattern is consistent with the relatively uniform decreases in light and moderate precipitation over the ocean. However, other spatial patterns of the trends in lapse rates in Fig. S7 bear little resemblance to the patterns in Fig. 4c, suggesting a secondary role for the reduction in lapse rate.

In summary, we find that the trends of regional annual total precipitation during the 1979–2013 warming period are

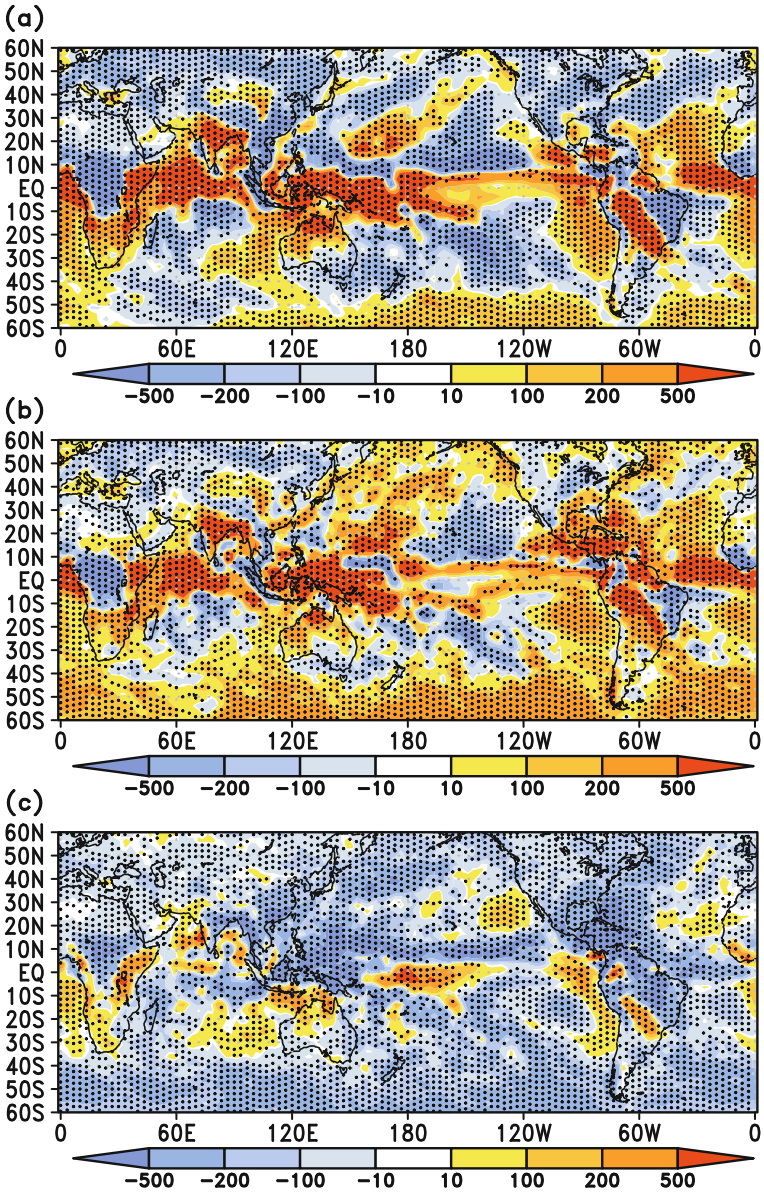

Fig. 4. (a) Trends in annual total precipitation (units: mm K^{-1}) in response to a one degree Kelvin warming in global mean temperature derived from MERRA reanalysis (1979–2013) by IDM. (b) As in (a) except for the top 30% heavy precipitation. (c) As in (a) except for the bottom 70% light and moderate precipitation. Crosses indicate changes significant at the 95% confidence level.

primarily controlled by the trends of the top 30% heavy precipitation, which in turn are driven by changes in precipitable water and the CMFMC in response to the warming. The trends of light and moderate precipitation are controlled by the compensating effect to heavy precipitation and, to a lesser degree, the reduction in lapse rate.

5. Widening of Hadley cells

The observed widening of Hadley cells is examined in Fig. 5b, where the trends of annual mean CMFMC (>20% K^{-1} increases in red dots, >20% K^{-1} decreases in blue dots) in response to a one degree Kelvin increase in global mean temperature derived from MERRA (1979–2013) are overlaid on the annual mean values of CMFMC averaged over the entire period of 1979–2013 (green shading). Figure 5c is the same as Fig. 5b, except for annual total precipitation. There is a high degree of consistency between Figs. 5b and c, and the widening of Hadley cells is unmistakable in both figures, especially in Fig. 5b. There are significant and extensive enhancements/expansions of precipitation centers (ascending/wet zones of Hadley cells) in the MC and Central America, and expansions of the tropical African rain belt to the east, south and west. There are only some minor exceptions, including relative minor decreases to the north of the tropical African rain belt, eastern South America, a tongue

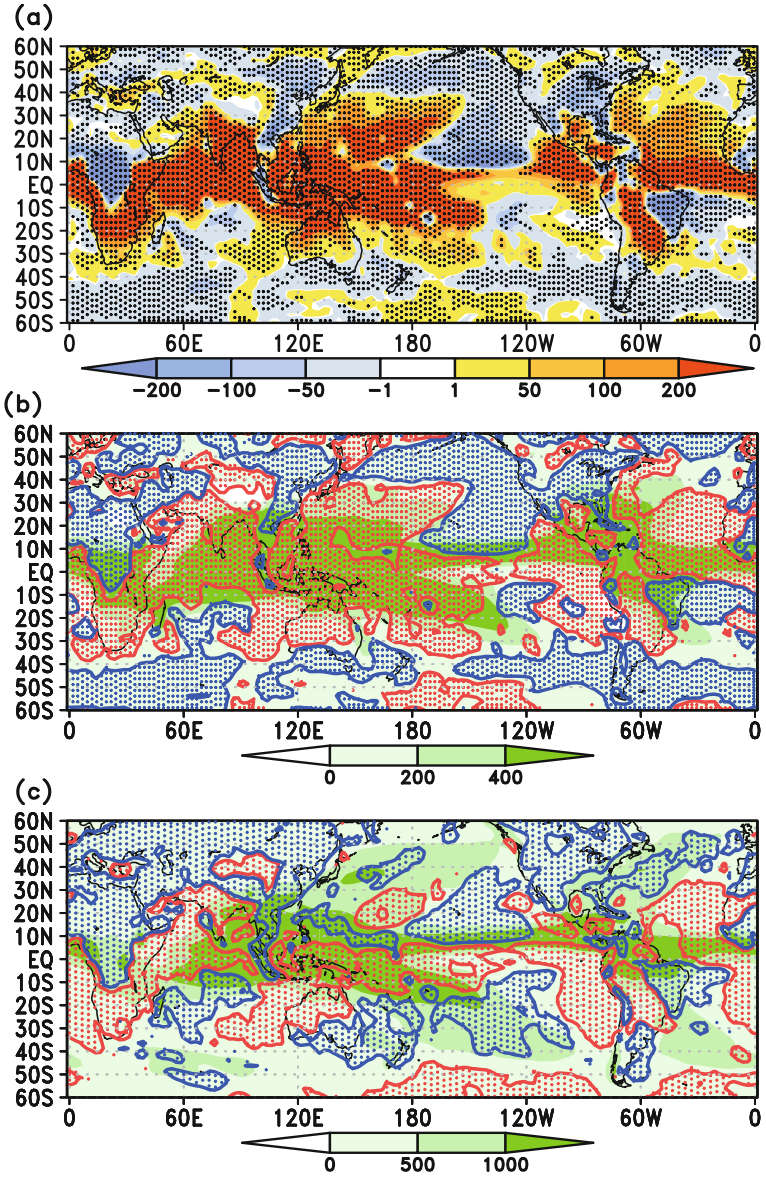

Fig. 5. (a) Trends in annual average upward moist convective mass flux (units: kg m^{-2} d^{-1} K^{-1}) at the 700 hPa pressure level in response to a one degree Kelvin global mean temperature increase derived from MERRA reanalysis (1979–2013). Crosses indicate changes significant at the 95% confidence level. (b) Percentage changes of the upward moist convective mass flux in response to a one degree Kelvin global temperature increase (in contours of $\pm$ 20% K^{-1}, red plus, blue minus) superposed on the upward moist convective mass (green shading) averaged over the entire period of 1979–2013. (c) As in (b) except for annual total precipitation.

from southern China to Southeast Asia, and a small tongue in the southern U.S. extending to the Caribbean. Meanwhile, there are widespread reductions of the CMFMC (Figs. 5a and b), as well as the annual total precipitation (Fig. 5c), in and around the descending/dry zones of Hadley cells; specifically, in the eastern Pacific, northern Africa, the Middle East, and southern Atlantic Ocean. These changes in ascending/wet zones and descending/dry zones of Hadley cells, which are consistent with the HHLL mechanism, constitute the expansion and enhancement of Hadley cells, in terms of the annual mean CMFMC as well as the annual total precipitation. As a result, there is a strengthening of the hydrological cycle in the near-global domain. These results are in good agreement with the observed widening of Hadley cells (Hu and Fu, 2007; Zhou et al., 2011; Davis and Rosenlof, 2012). Accordingly, we propose that the HHLL mechanism is the driving force for the widening of Hadley cells and the associated strengthening of the hydrological cycle in the near-global domain during the 1979–2013 global warming period.

The expansion and enhancement in Hadley cells can have

an important implication for Walker circulations. Enhancement of Hadley cells alone should strengthen Walker circulation, but expansion of Hadley cells as shown in Figs. 5b and c can shift the positions of both ascending and descending zones of Walker circulations, making the interpretation of trends in Walker circulation difficult. For instance, the Pacific Walker ascending zone shows an overwhelming enhancement and expansion of the CMFMC within the 110°–180°E longitudinal region of the tropics (30°S–30°N) (Figs. 5a and b), which expands primarily eastward, coupled with a moderate reduction in the CMFMC within 160°–120°W in the descending zone (blue dots), which is shifted obviously westward and northward (see also Fig. 5c). It follows that there is a strengthening of the Pacific Walker circulation in response to the global warming of 1979–2013 [in agreement with Zhou et al. (2011)]; however, the ascending zone moves significantly closer to the descending zone. Furthermore, the interpretation of the trends in the Pacific Walker circulation would be different if annual total precipitation (Fig. 5c), instead of the CMFMC (Figs. 5a or b), is used. The former is more sensitive to the latitudes used to study the Walker circulation (Zhao and Moore, 2008; Yu and Zwiers, 2010; Zhou et al., 2011).

Regarding the WWDD mechanism, Fig. 5c shows that significant increases and reductions of precipitation occur in both dry areas (<500 mm) and wet areas (>1000 mm), leaving the WWDD mechanism in doubt. Specifically, in wet regions of >1000 mm precipitation, the ratio of (>20% K^{-1} increase areas)/(>20% K^{-1} reduction areas) is about 3:2. Moreover, in the dry regions (<500 mm) of the Southern Hemisphere, there are larger areas of >20% K^{-1} increases than areas of >20% K^{-1} reductions.

6. Effects on water resources

Changes in precipitation are critical to water resources. We identify significant changes in Fig. 5c by a simple robustness test: regions of >20% K^{-1} changes in Fig. 5c that meet the 95% confidence level criterion (areas with crosses) in both Figs. 2a and 4a. Over land, changes meeting the robustness criterion include increasing precipitation in northern Australia, southern Africa, western India and western China. These are all located in dry areas with annual precipitation less than 500 mm, and thus will benefit from increasing water resources in response to global warming. The occurrence of these significant increases in precipitation in dry regions provides specific evidence against the WWDD theory. In fact, as discussed in the previous section, these four areas of increases are all due to the enhancements/expansions of tropical precipitation centers (ascending/wet zones of Hadley cells) in the MC and tropical Africa.

The areas of significant reductions in annual total precipitation over land meeting the robustness criterion include most of the U.S. and eastern Canada, the Middle East (ranging from Libya to Iran), and eastern South America. These areas would suffer greater scarcity of water resources due to global warming. All three areas can be attributed to the expansion of descending/dry zones of Hadley cells (Figs. 5b and c). Specifically, the U.S./Canada is part of the expansion of the descending zone of the Hadley cell in the eastern north Pacific; the Middle East is part of the expansion of the descending zone in North Africa/the eastern Atlantic Ocean; and eastern South America is part of the expansion of the descending zone in the southern Atlantic Ocean. Thus, the occurrence of these three reduction areas can also be attributed to the HHLL mechanism.

The drying of most of the U.S. found here provides observational support for the result reported by Seager et al. (2007), who found a broad consensus among climate models that this region will turn drier in the 21st century, and that the transition to a more arid climate should already be underway.

7. Limitations

An important limitation of the findings reported above is that our study is based on data from GPCP V2.2 and MERRA reanalysis for the time period 1979–2013. While our general conclusions on the HHLL mechanism and the enhancements and expansions of the three major tropical precipitation centers should be robust, our findings on the trends of specific regional precipitation may not be applicable to other periods of global warming, because the spatial distribution of the warming during 1979–2013 is significantly different from other historical periods global warming in the last 100 years (Hartmann et al., 2013). For instance, the spatial distributions of the warming in the periods 1951–80 and 1911–40 are remarkably different from that of 1981–2012, as shown in Hartmann et al. (2013, Fig. 2.22). To address this problem, we analyze gauge data over land from GPCC (Schneider et al., 2014) for the periods 1911–40 and 1951–80. The results on the trends in total precipitation, the top 30% heavy precipitation, and the bottom 70% light and moderate precipitation, are shown in Figs. S8 and S9. In the context of the controlling mechanism for the trends of regional precipitation in response to global warming, it is reassuring to see that Figs. S8 and S9 reconfirm the HHLL mechanism, as the trends in total precipitation (Figs. S8a and S9a) are closely matched by those in the top 30% heavy precipitation (Figs. S8b and S9b). Likewise, the negative (opposite in sign) mirroring characteristics between the top 30% heavy precipitation and the bottom 70% light and moderate precipitation are also very similar. This is particularly significant given that the spatial distributions of the warming in 1951–80 and 1911–40 are substantially different from those in 1979–2013 (Hartmann et al., 2013). Regarding the specific spatial distributions of the trends in regional precipitation, as expected, the trends of the 1911–40 period are reasonably consistent with those of the 1979–2013 period, while the trends of the 1951–1980 period are significantly different. For example, the reduction in annual mean precipitation over most of the U.S. is also present in the 1911–40 period, but is inverted (becomes wetter) in the 1951–80 period.

8. Summary

In this study, IDM is used to derive the trends of regional precipitation from observed GPCP and MERRA reanalysis data in the near-global domain of 60°S–60°N during the major global warming period of 1979–2013. We find that the trends of regional annual precipitation are primarily driven by the HHLL mechanism, rather than the WWDD mechanism. Specifically, the primary driving force is the changes in the top 30% heavy precipitation, which in turn are controlled by changes in precipitable water in response to global warming, i.e., by thermodynamic processes.

During the 1979–2013 warming period, we also find that there are extensive enhancements and expansions of the three major tropical precipitation centers (the MC, Central America, and tropical Africa), leading to the observed widening of Hadley cells and a significant strengthening of the global hydrological cycle. This suggests an enhancement, instead of a weakening, of Walker cells. Regionally, significant drying trends are found in most of the U.S. and eastern Canada, the Middle East, and eastern South America, while significant increases in precipitation occur in northern Australia, southern Africa, western India and western China.

Acknowledgements. This work was supported in part by the Chinese Academy of Sciences Strategic Priority Research Program (Grant No. XDB05010500), the Clean Air Research Project in China (Grant No. 201509001), and the Sustainable Development Research Project of Academia Sinica, Consortium for Climate Change Study, funded by the National Science Council (Grant No. 100-2119-M-001-029-MY5). This work was sponsored by the Collaborative Innovation Center for Regional Environmental Quality and the State Key Joint Laboratory of Environmental Simulation and Pollution Control, Peking University. The GPCC precipitation data were provided by NOAA/OAR/ESRL PSD, Boulder, Colorado, USA, via http://www.esrl.noaa.gov/psd/. We acknowledge the Global Precipitation Analysis, Laboratory for Atmospheres, NASA Goddard Space Flight Center (http://precip.gsfc.nasa.gov/) for providing the GPCP data, and the GMAO (Global Modeling and Assimilation Office) and GES DISC (Goddard Earth Sciences Data and Information Services Center) for providing the MERRA reanalysis dataset. We also thank You-Yu MAO and Chih-Wei WAN for their assistance with the data analysis. Finally, we are grateful to the two anonymous reviewers for their thoughtful reviews and advice, which led to an improved revised manuscript.

Electronic supplementary material: Supplementary material is available in the online version of this article at http://dx.doi.org/10.1007/s00376-015-5117-4.

REFERENCES

Adler, R. F., G. J. Gu, J. J. Wang, G. J. Huffman, S. Curtis, and D. Bolvin, 2008: Relationships between global precipitation and surface temperature on interannual and longer timescales (1979–2006). *J. Geophys. Res.*, **113**, D22104, doi: 10.1029/2008jd010536.

Adler, R. F., and Coauthors, 2003: The version-2 global precipitation climatology project (GPCP) monthly precipitation analysis (1979–present). *Journal of Hydrometeorology*, **4**, 1147–1167, doi: 10.1175/1525-7541(2003)004<1147:Tvgpcp>2.0.Co;2.

Allen, M. R., and W. J. Ingram, 2002: Constraints on future changes in climate and the hydrologic cycle. *Nature*, **419**, 224–232, doi: 10.1038/nature01092.

Chadwick, R., I. Boutle, and G. Martin, 2013: Spatial patterns of precipitation change in CMIP5: Why the rich do not get richer in the tropics. *J. Climate*, **26**, 3803–3822, doi: 10.1175/jcli-d-12-00543.1.

Chou, C., J. C. H. Chiang, C. W. Lan, C. H. Chung, Y. C. Liao, and C. J. Lee, 2013: Increase in the range between wet and dry season precipitation. *Nature Geoscience*, **6**, 263–267, doi: 10.1038/ngeo1744.

Cubasch, U., and Coauthors, 2001: Projections of future climate change. Chapter 9, *Climate Change 2001: The Scientific Basis. Contribution of Working Group I to the Third Assessment Report of the Intergovernmental Panel on Climate Change*, J. T. Houghton et al., Eds., Cambridge University Press, 524–582.

Dai, A. G., J. H. Wang, P. W. Thorne, D. E. Parker, L. Haimberger, and X. L. Wang, 2011: A new approach to homogenize daily radiosonde humidity data. *J. Climate*, **24**, 965–991, doi: 10.1175/2010jcli3816.1.

Davis, S. M., and K. H. Rosenlof, 2012: A multidiagnostic intercomparison of tropical-width time series using reanalyses and satellite observations. *J. Climate*, **25**, 1061–1078, doi: 10.1175/jcli-d-11-00127.1.

Dessler, A. E., and S. M. Davis, 2010: Trends in tropospheric humidity from reanalysis systems. *J. Geophys. Res.*, **115**, D19127, doi: 10.1029/2010jd014192.

Durre, I., C. N. Williams Jr., X. G. Yin, and R. S. Vose, 2009: Radiosonde-based trends in precipitable water over the Northern Hemisphere: An update. *J. Geophys. Res.*, **114**, D05112, doi: 10.1029/2008jd010989.

Hartmann, D. L., and Coauthors, 2013: Observations: Atmosphere and surface. Chapter 2, *Climate Change 2013: The Physical Science Basis. Contribution of Working Group I to the Fifth Assessment Report of the Intergovernmental Panel on Climate Change*, T. F. Stocker et al., Eds., Cambridge University Press, 159–254.

Held, I. M., and B. J. Soden, 2006: Robust responses of the hydrological cycle to global warming. *J. Climate*, **19**, 5686–5699, doi: 10.1175/jcli3990.1.

Hu, Y., and Q. Fu, 2007: Observed poleward expansion of the Hadley circulation since 1979. *Atmospheric Chemistry and Physics*, **7**, 5229–5236, doi: 10.5194/acp-7-5229-2007.

Jones, P. D., and A. Moberg, 2003: Hemispheric and large-scale surface air temperature variations: An extensive revision and an update to 2001. *J. Climate.*, **16**, 206–223, doi: 10.1175/1520-0442(2003)016<0206:HALSSA>2.0.CO;2.

Lau, K. M., and H. T. Wu, 2011: Climatology and changes in tropical oceanic rainfall characteristics inferred from Tropical Rainfall Measuring Mission (TRMM) data (1998–2009). *J. Geophys. Res.*, **116**, D17111, doi: 10.1029/2011jd015827.

Liu, C. L., and R. P. Allan, 2013: Observed and simulated precipitation responses in wet and dry regions 1850–2100. *Environmental Research Letters*, **8**, doi: 10.1088/1748-9326/8/3/034002.

Liu, S. C., C. B. Fu, C. J. Shiu, J. P. Chen, and F. T. Wu, 2009: Temperature dependence of global precipitation extremes. *Geo-*

phys. Res. Lett., **36**, L17702, doi: 10.1029/2009gl040218.

Mitchell, J. F. B., C. A. Wilson, and W. M. Cunnington, 1987: On CO_2 climate sensitivity and model dependence of results. *Quart. J. Roy. Meteor. Soc.*, **113**, 293–322, doi: 10.1002/qj.49711347517.

Mitchell, T. D., and P. D. Jones, 2005: An improved method of constructing a database of monthly climate observations and associated high-resolution grids. *Int. J. Climatol.*, **25**, 693–712, doi: 10.1002/joc.1181.

Rienecker, M. M., and Coauthors, 2011: MERRA: NASA's modern-era retrospective analysis for research and applications. *J. Climate*, **24**, 3624–3648, doi: 10.1175/Jcli-D-11-00015.1.

Santer, B. D., and Coauthors, 2007: Identification of human-induced changes in atmospheric moisture content. *Proc. Natl. Acad. Sci. USA*, **104**, 15248–15253, doi: 10.1073/pnas.0702872104.

Schneider, U., A. Becker, P. Finger, A. Meyer-Christoffer, M. Ziese, and B. Rudolf, 2014: GPCC's new land surface precipitation climatology based on quality-controlled in situ data and its role in quantifying the global water cycle. *Theor. Appl. Climatol.*, **115**, 15–40, doi: 10.1007/s00704-013-0860-x.

Seager, R., and Coauthors, 2007: Model projections of an imminent transition to a more arid climate in southwestern North America. *Science*, **316**, 1181–1184, doi: 10.1126/science.1139601.

Shiu, C. J., S. C. Liu, C. B. Fu, A. G. Dai, and Y. Sun, 2012: How much do precipitation extremes change in a warming climate? *Geophys. Res. Lett.*, **39**, L17707, doi: 10.1029/2012gl052762.

Smith, T. M., R. W. Reynolds, T. C. Peterson, and J. Lawrimore, 2008: Improvements to NOAA's historical merged land–ocean surface temperature analysis (1880–2006). *J. Climate*, **21**, 2283–2296, doi: 10.1175/2007jcli2100.1.

Stachnik, J. P., and C. Schumacher, 2011: A comparison of the Hadley circulation in modern reanalyses. *J. Geophys. Res.*, **116**, D22102, doi: 10.1029/2011jd016677.

Sun, Y., S. Solomon, A. G. Dai, and R. W. Portmann, 2007: How often will it rain? *J. Climate*, **20**, 4801–4818, doi: 10.1175/jcli4263.1.

Tokinaga, H., S. P. Xie, C. Deser, Y. Kosaka, and Y. M. Okumura, 2012: Slowdown of the Walker circulation driven by tropical Indo-Pacific warming. *Nature*, **491**, 439–444, doi: 10.1038/nature11576.

Trenberth, K. E., A. G. Dai, R. M. Rasmussen, and D. B. Parsons, 2003: The changing character of precipitation. *Bull. Amer. Meteorol. Soc.*, **84**, 1205–1217, doi: 10.1175/bams-84-9-1205.

Trenberth, K. E., J. Fasullo, and L. Smith, 2005: Trends and variability in column-integrated atmospheric water vapor. *Climate Dyn.*, **24**, 741–758, doi: 10.1007/s00382-005-0017-4.

Trenberth, K. E., and Coauthors, 2007: Observations: surface and atmospheric climate change. Chapter 9, *Climate Change 2007: The Physical Science Basis. Contribution of Working Group I to the Fourth Assessment Report of the Intergovernmental Panel on Climate Change*, S. Solomon et al., Eds., Cambridge University Press, 747–845.

Vecchi, G. A., and B. J. Soden, 2007: Global warming and the weakening of the tropical circulation. *J. Climate*, **20**, 4316–4340, doi: 10.1175/jcli4258.1.

Vecchi, G. A., B. J. Soden, A. T. Wittenberg, I. M. Held, A. Leetmaa, and M. J. Harrison, 2006: Weakening of tropical Pacific atmospheric circulation due to anthropogenic forcing. *Nature*, **441**, 73–76, doi: 10.1038/nature04744.

Vose, R. S., R. L. Schmoyer, P. M. Steurer, T. Peterson, R. Heim, T. Karl, and J. Eischeid, 1992: *The Global Historical Climatology Network: Long–Term Monthly Temperature, Precipitation, Sea Level Pressure, and Station Pressure Data*. Carbon Dioxide Information Analysis Center, Oak Ridge National Laboratory, Oak Ridge, TN., 325 pp, doi: 10.3334/CDIAC/cli.ndp041.

Yu, B., and F. W. Zwiers, 2010: Changes in equatorial atmospheric zonal circulations in recent decades. *Geophys. Res. Lett.*, **37**, L05701, doi: 10.1029/2009gl042071.

Zhao, H. X., and G. W. K. Moore, 2008: Trends in the boreal summer regional Hadley and Walker circulations as expressed in precipitation records from Asia and Africa during the latter half of the 20th century. *International Journal of Climatology*, **28**, 563–578, doi: 10.1002/Joc.1580.

Zhou, Y. P., K. M. Xu, Y. C. Sud, and A. K. Betts, 2011: Recent trends of the tropical hydrological cycle inferred from Global Precipitation Climatology Project and International Satellite Cloud Climatology Project data. *J. Geophys. Res.*, **116**, D09101, doi: 10.1029/2010jd015197.